The Abundance of Atomic Sulfur in the Atmosphere of Io

Lori M. Feaga[1], Melissa A. McGrath[2], and Paul D. Feldman[1]

ABSTRACT

Observations with the Space Telescope Imaging Spectrograph aboard the Hubble Space Telescope have been used to constrain the atomic sulfur column density in Io's atmosphere. The S I λ1479 dipole allowed and forbidden transition multiplets have been resolved for the first time at Io, enabling the study of both optically thick and thin transitions from a single atomic species. The allowed transitions contribute 62 $\pm$ 8% and the forbidden transitions 38 $\pm$ 8%, on average, to the total signal of the S I λ1479 multiplets. Using the optically thick and thin transitions of S I λ1479 observed near the limbs of Io, we derive a tangential atmospheric sulfur column abundance of $3.6\times10^{12}\,\mathrm{cm}^{-2} < \mathcal{N}_s < 1.7\times10^{13}\,\mathrm{cm}^{-2}$, which is independent of electron temperature and density. A low density SO_2 atmosphere, $\mathcal{N}_{so_2} \sim 5\text{-}10\times10^{15}\,\mathrm{cm}^{-2}$, consistent with that inferred from other recent observations, is most consistent with these bounds.

Subject headings: planets and satellites: individual (Io)—ultraviolet: solar system—atomic data

1. Introduction

Io's atmosphere plays a key role in populating the jovian magnetosphere with plasma and replenishing the plasma torus with sulfur and oxygen (Spencer & Schneider 1996). This tenuous atmosphere, first detected by the Voyager 1 IRIS experiment over 20 years ago (Pearl et al. 1979), has proven to be a challenge to characterize quantitatively. It is composed primarily of SO_2 (Lellouch et al. 1990, 1992) and SO (Lellouch et al. 1996). The atomic by-products of SO_2, sulfur and oxygen, were first identified in the Io plasma torus (Brown 1981; Durrance, Feldman, & Weaver 1983), and more recently detected in Io's emission line spectrum (Ballester et al. 1987). Sodium (Burger & Schneider 1998; Geissler et al. 1999; Bouchez, Brown, & Schneider 2000) and potassium (Brown 2001) are also present at much lower abundance than sulfur and oxygen. The observed emissions are produced when the atmospheric sulfur and oxygen are collisionally excited by impinging electrons from the plasma torus. The emissions are therefore diagnostic of the plasma interaction with Io's atmosphere, providing quantitative information about the electron temperature and density, in addition to the abundances of sulfur and oxygen.

Despite the recent advances in quantifying Io's atmosphere, including investigating the inhomogeneity and impact of volcanic activity (Feldman et al. 2000; McGrath et al. 2000; Spencer et al. 2000), analyzing the airglow (Geissler et al. 1999), and resolving the morphology (Roesler et al. 1999; Retherford et al. 2000), and the fact that several sets of sulfur and oxygen emission line data have been acquired and analyzed (Ballester 1989; McGrath et al. 2000; Oliversen et al. 2001; Wolven et al. 2001), the abundances are still not well constrained. Various observational measurements and theoretical models have placed loose bounds on the sulfur column density ($\mathcal{N}_s$). Previously, electron densities and temperatures were assumed in order to estimate $\mathcal{N}_s$, resulting in limits of $2.2\times10^{12}\,\mathrm{cm}^{-2} < \mathcal{N}_s < 7\times10^{15}\,\mathrm{cm}^{-2}$ (Ballester et al. 1987; McGrath et al. 2000). Recent observations make both optically thick and optically thin regimes available in a single exposure, allowing us to constrain $\mathcal{N}_s$ without assuming a specific T_e or n_e. We present such a temperature and density independent method for determining the column density in this paper.

Sulfur and oxygen abundances also provide a little-utilized diagnostic of the origin and nature of the SO_2

[1]Department of Physics and Astronomy, Johns Hopkins University, 3400 N. Charles Street, Baltimore, MD 21218; lanier@pha.jhu.edu, pdf@pha.jhu.edu

[2]Space Telescope Science Institute, 3700 San Martin Drive, Baltimore, MD 21218; mcgrath@stsci.edu

atmosphere. Significant progress has been made in characterizing both the spatial distribution and temporal variability of the SO_2 atmosphere (Ballester et al. 1994; Trafton et al. 1996; McGrath et al. 2000; Feldman et al. 2000; Spencer et al. 2000; Strobel & Wolven 2001). The current picture includes a higher column density equatorial, sub-solar region, $\mathcal{N}_{so_2} \sim$ 1-5$\times 10^{16}$ cm^{-2}, with a strong poleward gradient, where $\mathcal{N}_{so_2}$ decreases to $< 10^{15}$ cm^{-2} (Feldman et al. 2000; Strobel & Wolven 2001) and column densities $> 10^{16}$ cm^{-2} above active volcanic regions (McGrath et al. 2000; Spencer et al. 2000). It is obvious that both active volcanism and SO_2 frost sublimation are important atmospheric sources, although the relative importance of each mechanism has not been determined (Summers & Strobel 1996; Wong & Smyth 2000; Moses, Zolotov, & Fegley 2001). The models show that sulfur can serve as a proxy for SO_2, with enhanced abundance relative to oxygen during and shortly after volcanic activity as compared to a sublimation atmosphere. Sulfur displays similar trends as, and scales well with, the SO_2 abundance in most of the dayside models. Determining and monitoring the sulfur abundance, can, in principle, provide a much-needed measure of the variability of Io's atmosphere.

We describe the observations and explain the data reduction in Section 2. We then give the motivation for and present the analysis of the opacity of the sulfur transitions and the atomic sulfur column density in Section 3. Finally, we discuss the implications of our findings in Section 4.

2. Observations and Data Reduction

The Space Telescope Imaging Spectrograph (STIS) aboard the Hubble Space Telescope (HST) has made it possible to study the sulfur emission near 1479 Å in detail. The allowed multiplet, S I λ1479 ($3s^2\,3p^3\,4s'\,{}^3D^0 \rightarrow 3s^2\,3p^4\,{}^3P$), and the intercombination multiplet, S I] λ1479 ($3s^2\,3p^3\,3d\,{}^5D^0 \rightarrow 3s^2\,3p^4\,{}^3P$), are both present in the data and are resolved for the first time. The analysis that follows focuses on the separation of the S I λ1479 multiplets and its implications. Additional data collected with the International Ultraviolet Explorer (IUE), from 1986-1988, and the Faint Object Spectrograph (FOS) on HST, from 1992-1996, are re-examined in light of the STIS data. We present only one representative spectrum per instrument in this paper. We concentrate specifically on the following sulfur emission multiplets: the intercombination and allowed multiplets at S I λ1479, the allowed multiplet S I λ1814 ($3s^2\,3p^3\,4s\,{}^3S^0 \rightarrow 3s^2\,3p^4\,{}^3P$), and the intercombination doublet S I] λ1900 ($3s^2\,3p^3\,4s\,{}^5S^0 \rightarrow 3s^2\,3p^4\,{}^3P$). For all but the 1479 Å multiplet, there are several years of data that confirm the trends and ratios found in our analysis. Table 1 summarizes the data analyzed, with the observations presented in this paper shown in bold. The morphology of the STIS observations is identical to that described in Retherford et al. (2000), with resolved bright auroral emission regions near the Io equator at both sub- and anti-Jupiter locations. The equatorial spots are not resolved in the other observations presented here.

The primary data set we analyze was acquired with STIS on HST using the $52'' \times 2''$ slit and the G140M grating, which produces a monochromatic image of Io at each emission line detected in the spectral range 1440-1500 Å. The set contains four $\sim$19 minute exposures taken on 1998 August 21-22 while Io was near western elongation, Io orbital longitude 285°-305°. The coadded flux spectrum of the first two exposures is presented in Figure 1. The data are acquired at a dispersion of 0.051 Å/pixel and spectral resolution of $\sim$ 0.5 Å, allowing 6 blended components of the S I λ1479 multiplets to be resolved. The detected features correspond to both the electric dipole allowed and forbidden transitions shown in the Grotrian diagram in Figure 2. Atomic data for the transitions are given in Table 2. The blended allowed transition wavelengths are 1474.1 Å, 1483.1 Å, and 1487.2 Å, while the blended forbidden transitions are at 1473.0 Å, 1481.7 Å, and 1485.6 Å.

These data were reduced in the following manner. The rectified (x2d) images were boxcar smoothed over a 3×3 pixel region and background subtracted. The wavelength dependent background level was determined by averaging the signal in a region spatially one Io diameter away from and comparable in size to the bright spectral features. Next, several rectangular sub-images, centered on the brightest emission areas of the anti- and sub-jovian equatorial features, were created in order to isolate these spots and to ensure no overlap of emission. Lastly, the data in the sub-images were compressed spatially into a one-dimensional array of flux vs. wavelength. Because the spots are not located at the center of the aperture, their flux spectra have systematic wavelength offsets, which we have corrected for. A Gaussian profile was fitted to each of the 6 resolved emission features to determine their relative strengths. These Gaussians are overplotted on the

data in Figure 3.

We re-analyze a set of IUE observations of Io which span the spectral range 1150-1950 Å (Ballester 1989). Low resolution ~ 5 Å exposures of 13-14 hours in length were made over a three year period with the short-wavelength (SWP) camera. We present a representative spectrum in Figure 4a which is centered on Io's western elongation on 1987 July 31; it was reduced following the same method as Ballester and smoothed using a 5-element boxcar routine. An additional step was taken to remove the reflected light continuum longward of 1700 Å by subtracting a solar spectrum scaled to the intensity of the underlying continuum.

The last set of Io observations we re-analyze was made with the FOS. These observations cover 1600-2300 Å and were obtained over a period of four years using the G190H grating, which has a dispersion of 1.45 Å/diode. Exposures varied in length between 10 and 20 minutes. The representative spectrum shown in Figure 4b was acquired while Io was emerging into sunlight from Jupiter's shadow on 1996 October 2. In order to minimize scattered light contamination, only the first 7 groups of the data, corresponding to Io in eclipse, were used. The data were reduced in the same manner as presented in McGrath et al. (2000) and were rebinned by 2 pixels and smoothed by 3.

Several factors were considered in the analysis, including the influence of the emission morphology on the results, and possible contamination from SO_2 absorption. The emission morphology (e.g., one or two spots visible) depends on Io's orbital geometry (Roesler et al. 1999; Retherford et al. 2000), which may affect the absolute magnitude of the measured fluxes. When Io is at western elongation, as it is for part of the IUE and all of the STIS integration time, both equatorial spots are in view for at least part of the exposure. For the FOS egress data, when Io is in shadow emerging from behind Jupiter, only one equatorial spot would be visible if resolved. We assume that the opacity and the S I λ1479 analysis we present are independent of the emission morphology. Concerning contamination due to SO_2 absorption, since the SO_2 is more concentrated at lower altitude than the atomic sulfur in the atmosphere, the absorption should be minimal. Also, at the relevant wavelengths, the average SO_2 transmission is close to unity. Therefore, the relative line strengths of the sulfur multiplets should not be significantly affected.

3. Analysis

3.1. Allowed and Forbidden Components of S I λ1479

It is desirable to separate the allowed from the forbidden transitions since the transition probabilities and the oscillator strengths for the two transitions are very different. The forbidden transitions are much more likely to be optically thin than the allowed ones, meaning two regimes of opacity can potentially be sampled. A quantitative determination of the relative contributions of the allowed and forbidden transitions can also be used to help analyze numerous data sets for which the multiplets are unresolved.

A synthetic sulfur emission spectrum is created for the STIS data set by adding together 13 Gaussians of the same FWHM, one at each of the central wavelengths of the components of the S I λ1479 multiplet. Each Gaussian is weighted by its optically thin relative strength as reported in Morton (1991) and then the entire synthetic spectrum is scaled to the intensity level of the data. A fit of the synthetic spectrum to the data is shown in Figure 3. The flux from each line is determined by integrating the area under the Gaussian curves in Figure 3 and is reported in Table 3. The allowed transitions contribute an average of $62 \pm 8\%$ and the forbidden transitions an average of $38 \pm 8\%$ to the total signal of the S I λ1479 emission. Although the anti- and sub-jovian equatorial spots differ in flux by up to a factor of 2, the relative line ratios and the contribution of the allowed and forbidden components are consistent throughout the data set.

3.2. Opacity of the Observed S I Emissions

A synthetic sulfur emission spectrum is also created for the IUE and FOS data sets. A unique FWHM is chosen for each data set to match the resolution of the instrument. Again, Gaussians are placed at the central wavelengths for all lines of a given sulfur multiplet, weighted by its optically thin relative strength (Morton 1991), and scaled to the data. If the data match the synthetic spectrum, sulfur is considered optically thin in that emission; otherwise, it is considered optically thick.

The fits for S I λ1814 and S I] λ1900 are overplotted on the data in Figure 4. If optically thin, the transitions of the S I λ1814 multiplet should be in a $5.2:3:1$ ratio and the S I] λ1900 doublet will be in a $3.6:1$ ratio. The ratios are calculated from their transi-

tion probabilities listed in Table 2. We observe a ratio of 3.4 : 5.6 : 1 and 4.5 : 5 : 1 for the 1814 multiplet using the IUE and FOS data respectively, and 3 : 1 and 3.4 : 1 in the 1900 doublet. Our results therefore indicate that the S I] λ1900 doublet is optically thin and the S I λ1814 multiplet is optically thick. Moreover, we have analyzed all the IUE and FOS data listed in Table 1 and find that in all existing observations of Io, the 1900 Å doublet is observed to be optically thin and the 1814 Å multiplet is observed to be optically thick.

The allowed transitions of the S I λ1479 multiplet have a theoretical ratio of 5.2 : 3.1 : 1 when optically thin (Morton 1991). We observe a ratio of 5.3 : 3.8 : 1 in the STIS data for the S I λ1479 allowed multiplet. Initially, our line ratios seemed to indicate that the S I λ1479 allowed multiplet is optically thin since the blended line ratios are consistent with the optically thin values; however, this contradicts the fact that the S I λ1814 multiplet, which has the same ground state and similar oscillator strength as S I λ1479, is consistently optically thick in all existing observations of Io. A more detailed analysis of the S I λ1479 allowed transitions shows that because the lines are blends at STIS resolution, optical depth effects can be hidden by the blending. The shorter wavelength transitions of a given blend, for example 1473.99 Å, 1474.38 Å, and 1483.04 Å, are preferentially depleted at high optical depth. The flux in these transitions is redistributed in the multiplet such that the fluxes in the longer wavelength transitions of the blend, 1474.57 Å and 1483.23 Å, are enhanced, and the 5 : 3 : 1 ratio of the blends is unaffected by this flux redistribution.

3.3. Constraints on $\mathcal{N}_s$

The optical depth of a transition is directly proportional to both the column density and the absorption cross section, $\tau = \mathcal{N}\sigma$, with τ = 1 serving as the conventional boundary between the optically thin and thick regimes. Therefore, generally speaking, an upper limit can be placed on the sulfur column density in the optically thin regime, and a lower limit in the optically thick regime. If σ is known, the sulfur column density can be constrained without assuming a specific T_e or n_e.

The absorption cross section of photons in the core of an optically thin transition where only thermal Doppler broadening and radiative damping are considered is directly proportional to the oscillator strength, f_{ij}, of the transition (Osterbrock 1989). Assuming τ = 1,

$$\mathcal{N} = \frac{1}{\sigma} = \frac{m_e c \Delta\nu_D}{\sqrt{\pi} e^2 f_{ij}} = \frac{m_e c}{\sqrt{\pi} e^2 f_{ij}} \sqrt{\frac{2kT}{m_s c^2}} \nu_o. \quad (1)$$

Several consistent values of the oscillator strength are published for the dipole allowed transitions S I λ1814 and S I λ1479. Only one value of the oscillator strength exists for the majority of the forbidden transitions of S I] λ1479. For the S I] λ1900 transition, only two values of the oscillator strengths and transition probabilities exist (Müller 1968; Tayal 1998–see the discussion in McGrath et al. (2000) on the order of magnitude disagreement between these values). The values and references for the transition probabilities and oscillator strengths we use are given in Table 2.

Using equation (1) with T = 1000K and the oscillator strength of f_{ij} = 0.090 (Morton 1991) for the S I λ1479 allowed multiplet, the lower bound for the sulfur column density is 3.6×10^{12} cm^{-2}. A similar lower bound of 2.8×10^{12} cm^{-2} is found using the f_{ij} value of 0.093 (Tayal 1998) for the S I λ1814 multiplet. An upper bound of 1.7×10^{13} cm^{-2} is found using the oscillator strength of the dominant S I] λ1479 forbidden transition line, 1472.97 Å, listed in Morton (1991) as f_{ij} = 0.019. This result is lower than the previous upper bound for the atomic sulfur column density at Io, 7×10^{15} cm^{-2}, by more than 2 orders of magnitude (McGrath et al. 2000). An explanation of this discrepancy is given in the discussion.

3.4. Constraints on T_e and n_e

Knowledge about the sulfur column density in turn allows us to place constraints on the electron temperature and density of the impacting plasma. The observed line of sight brightness is given by

$$B_{ij} = \int n_s n_e Q_{ij}(T_e) dl \quad (2)$$

where n_s and n_e are the sulfur and electron densities, respectively, and $Q_{ij}(T_e)$ is the temperature dependent electron excitation rate coefficient. Although it has been shown by Combi et al. (1998) and Saur et al. (1999) that the plasma flow and interaction around Io creates varying electron density and temperature profiles at Io, we assume that n_e and T_e are constant along the line of sight, invert equation (2), and arrive at an approximate relationship between the sulfur column density and the measured emission line brightness,

$$\mathcal{N} \sim \frac{10^6\, B_{ij}}{\overline{n}_e\, Q_{ij}(\overline{T}_e)} \quad (cm^{-2}) \quad (3)$$

where B_{ij} is in units of Rayleighs, $\overline{n}_e$ is in units of cm^{-3}, and Q_{ij} is in units of cm^3 s^{-1}. For a particular transition from an upper state j to a lower state i, the rate coefficient is (Osterbrock 1989)

$$Q_{ij}(\overline{T}_e) = \frac{8.63 \times 10^{-6}\, \overline{\Omega}_{ij} e^{-E_{ij}/kT_e}}{\omega_i \sqrt{\overline{T_e}}}, \qquad (4)$$

where $\overline{\Omega}_{ij}$ is the thermally averaged collision strength, ω_i is the statistical weight of the lower state, E_{ij} is the transition energy in units of eV, k is the Boltzmann constant, and T_e is the electron temperature in units of Kelvin. These equations apply only to optically thin transitions, therefore, the S I] λ1479 forbidden multiplet or the S I] λ1900 intercombination doublet must be used in determining the electron temperature and density. As there are no electron impact excitation cross-sections or collision strengths available for the S I] λ1479 forbidden multiplet, the S I] λ1900 intercombination doublet is used for the analysis. We use the electron excitation rate presented in Figure 9a of McGrath et al. (2000).

Combining the sulfur column density bounds from the S I λ1479 analysis, the line brightnesses of the S I] λ1900 intercombination doublet from the IUE data when Io was west of Jupiter, and equation (3), the density and temperature of the impacting electrons can be estimated. For an electron temperature range of 0.8-100 eV and several impacting electron density values between 500 and 10000 cm^{-3}, the column density is plotted in Figure 5. Both a low temperature solution, 1.5 eV $< T_e <$ 7 eV, and a high temperature solution, 7 eV $< T_e <$ 100 eV, are possible. The canonical values of 5 eV and 2000 cm^{-3} are consistent with the low temperature solution. Assuming the low temperature solution implies 1000 cm^{-3} $< n_e <$ 5000 cm^{-3}.

4. Discussion

The STIS observations presented here and used to calculate the atomic sulfur column density are tangential cuts through Io's atmosphere centered on the equatorial spots; therefore, the column densities are also tangential. Wolven et al. (2001) has recently published a collection of four years of HST/STIS low resolution observations of near Io emissions and extended emissions in the 1150-1730 Å wavelength range. The photon fluxes measured at 1 Io radius for the S I λ1479 multiplets varied between 3×10^{-4} cm^{-2} sec^{-1} and 3×10^{-3} cm^{-2} sec^{-1}, corresponding to eclipse and western elongation, respectively. These values are consistent with our HST/STIS photon fluxes for S I λ1479, implying that the tangential sulfur column that Wolven et al. (2001) were sampling should have values for $\mathcal{N}_s$ similar to ours. McGrath et al. (2000) determined the vertical column density of S, SO, and SO_2 above specific locations on Io, including the Pele volcano. With an estimated collision strength and electron impact excitation rate coefficient for the S I] λ1900 doublet, and assuming canonical plasma torus values of electron density and temperature, 1000 cm^{-3} and 5 eV, they determine an $\mathcal{N}_s$ of 1×10^{14} cm^{-2} at Pele, which is much larger than our upper bound of 1.3×10^{13} cm^{-2}. A column density that is significantly larger than our value should result in additional optical depth effects. In Figure 6, the Pele flux spectrum published in Figure 2 of McGrath et al. (2000) is compared with the optically thin FOS synthetic spectrum described earlier, and confirms that the S I λ1814 multiplet is more optically thick over Pele than in our IUE and FOS spectra, lending credence to the significantly higher value of $\mathcal{N}_s$ over Pele despite the uncertainty in the S I] λ1900 electron excitation rate. This implies that $\mathcal{N}_s$ is larger in volcanic plumes than in the equatorial spots.

In the 1-D, steady state photochemical atmospheric models presented by Summers & Strobel (1996), both high and low density SO_2 atmosphere sub-solar profiles with various levels of vertical eddy mixing are calculated. We have extracted the vertical column densities of several atmospheric components from their published profiles. The $\mathcal{N}_s$ values corresponding to the high density SO_2 cases, $\mathcal{N}_{so_2}$ = 10^{18} cm^{-2}, were much higher than the limits from our analysis. For example, with a low vertical eddy mixing coefficient of k = 10^6 cm^2 sec^{-1}, $\mathcal{N}_s \sim 2\times10^{17}$ cm^{-2}; for a high vertical eddy mixing coefficient of k = 10^9 cm^2 sec^{-1}, $\mathcal{N}_s \sim 9\times10^{14}$ cm^{-2}. On the other hand, for their low density case ($\mathcal{N}_{so_2}$ = 8×10^{15} cm^{-2} with high eddy mixing k = 10^9 cm^2 sec^{-1}) $\mathcal{N}_s \sim 6\times10^{12}$ cm^{-2}. The corresponding tangential column density, assuming spherical symmetry and using the atmospheric sulfur number density profile in Summers & Strobel (1996), is on the order of 4×10^{13} cm^{-2}. This value is much more consistent with our results and the general overall picture of the SO_2 atmosphere described in the introduction. In a 3-D high density SO_2 model atmosphere presented by Wong & Smyth (2000), they assume an initial sub-solar $\mathcal{N}_{so_2}$ of 6×10^{17} cm^{-2}, which results in a tangential sulfur column density at the terminator, $\mathcal{N}_s \sim 2\times10^{15}$ cm^{-2}, inconsistent with our upper limit

to $\mathcal{N}_s$. In the model in which the input SO_2 column is reduced to a lower density value of 7×10^{16} cm^{-2}, the tangential $\mathcal{N}_s$ is more consistent with our results at a value of 6×10^{13} cm^{-2}.

In order to predict what the atmospheric driving mechanism is, Moses, Zolotov, & Fegley (2001) have modeled both an SO_2 frost sublimation atmosphere and a Pele-type volcanically driven atmosphere. Of the two models, our $\mathcal{N}_s$ value is more consistent with the SO_2 frost sublimation atmosphere simply because this model has a lower sulfur column density. However, the true test to the Moses et al. (2001) models is to compare the sulfur to oxygen column abundances extracted from a single exposure. When the sulfur is more abundant than the oxygen, the models imply a volcanically driven atmosphere. None of the medium resolution data presented here had a simultaneous oxygen detection, so the ratio is not currently available, although this sulfur to oxygen relationship will be analyzed in future work with a more extensive data set.

The authors would like to thank Darrell Strobel and Warren Moos for insightful discussions on the atomic physics of the UV sulfur transitions. We are also grateful to Brian Wolven and Kurt Retherford for help with the STIS data reduction. Support for this work was provided by NASA through grant number HST-AR-09211.01-A from the Space Telescope Science Institute, which is operated by the Association of Universities for Research in Astronomy, Incorporated, under NASA contract NAS5-26555.

REFERENCES

Ballester, G. E. 1989, Ultraviolet observations of the atmosphere of Io, PhD thesis, Dept. of Physics and Astronomy, The Johns Hopkins University

Ballester, G. E., et al. 1987, ApJ, 319, L33

Ballester, G. E., McGrath, M. A., Strobel, D. F., Zhu, X., Feldman, P. D., & Moos, H. W. 1994, Icarus, 111, 2

Bouchez, A. H., Brown, M. E., & Schneider, N. M. 2000, Icarus, 148, 316

Brown, M. E. 2001, Icarus, 151, 190

Brown, R. A. 1981, ApJ, 244, 1072

Burger, M. H., & Schneider, N. M. 1998, BAAS, 30, 1390

Combi, M. R., Kabin, K., Gombosi, T. I., DeZeeuw, D. L., & Powell, K. G. 1998, J. Geophys. Res., 103, 9071

Durrance, S. T., Feldman, P. D., & Weaver, H. A. 1983, ApJ, 267, L125

Feldman, P. D., et al. 2000, Geophys. Res. Lett., 27, 1787

Geissler, P. E., McEwen, A. S., Ip, W., Belton, M. J. S., Johnson, T. V., Smyth, W. H., & Ingersoll, A. P. 1999, Science, 285, 870

Lellouch, E., Belton, M. J. S., de Pater, I., Gulkis, S., & Encrenaz, T. 1990, Nature, 346, 639

Lellouch, E., Belton, M. J. S., de Pater, I., Paubert, G., Gulkis, S., & Encrenaz, T. 1992, Icarus, 98, 271

Lellouch, E., Strobel, D. F., Belton, M. J. S., Summers, M. E., Paubert, G., & Moreno, R. 1996, ApJ, 459, L107

McGrath, M. A., Belton, M. J. S., Spencer, J. R., & Sartoretti, P. 2000, Icarus, 146, 476

Morton, D. C. 1991, ApJS, 77, 119

Moses, J. I., Zolotov, M. Y., & Fegley, B. 2001, Icarus, in press

Müller, D. 1968, Z. Nature, 23A, 1707

Oliversen, R. J., Scherb, F., Smyth, W. H., Freed, M. E., Woodward, R. C., Marconi, M. L., Retherford, K. D., Lupie, O. L., & Morgenthaler, J. P. 2001, J. Geophys. Res., 106, 26183

Osterbrock, D. E. 1989, Astrophysics of Gaseous Nebulae and Active Galactic Nuclei (Mill Valley: University Science Books)

Pearl, J., Hanel, R., Kunde, V., Maguire, W., Fox, K., Gupta, S., Ponnamperuma, C., & Raulin, F. 1979, Nature, 280, 755

Retherford, K. D., Moos, H. W., Strobel, D. F., Wolven, B. C., & Roesler, F. L. 2000, J. Geophys. Res., 105, 27157

Roesler, F. L., et al. 1999, Science, 283, 353

Saur, J., Neubauer, F. M., Strobel, D. F., & Summers, M. E. 1999, J. Geophys. Res., 104, 25105

Spencer, J. R., Jessup, K. L., McGrath, M. A., Ballester, G. E., & Yelle, R. 2000, Science, 288, 1208

Spencer, J. R., & Schneider, N. M. 1996, Annu. Rev. Earth Planet. Sci., 24, 125

Strobel, D. F., & Wolven, B. C. 2001, Ap&SS, 277, 271

Summers, M. E., & Strobel, D. F. 1996, Icarus, 120, 290

Tayal, S. S. 1998, ApJ, 497, 493

Trafton, L. M., Caldwell, J. J., Barnet, C., & Cunningham, C. C. 1996, ApJ, 456, 384

Wolven, B. C., Moos, H. W., Retherford, K. D., Feldman, P. D., Strobel, D. F., Smyth, W. H., & Roesler, F. L. 2001, J. Geophys. Res., 106, 26155

Wong, M. C., & Smyth, W. H. 2000, Icarus, 146, 60

AAS LaTeX macros v5.0.

TABLE 1
SUMMARY OF IO OBSERVATIONS

Observation	UT Date	UT Time (hh:mm(:ss))	Io Diameter (″)	Exposure Time (s)
		IUE		
swp28708	1986 Jul 18	21:49	1.14	48600
swp29430	1986 Oct 12	15:29	1.21	49800
swp31440	**1987 Jul 31**	**18:53**	**1.06**	**50400**
swp31447	1987 Aug 1	16:57	1.07	48000
swp34341	1988 Sep 27	17:02	1.12	48600
swp34343	1988 Sep 28	14:49	1.12	47700
		HST/FOS		
y0w00203-4	1992 Mar 22	13:18:10	1.11	1680
y0w05402	1992 May 16	10:17:41	0.97	1245
y1a10801	1993 Aug 4	02:44:55	0.84	851
y2wta201	1995 Oct 9	12:48:19	0.86	738
y3cwb101-5	1996 Aug 1	07:20:06	1.17	4920
y3eta201	**1996 Oct 2**	**19:24:22**	**0.98**	**800**
		HST/STIS		
o4xm03050	**1998 Aug 21**	**22:07:17**	**1.23**	**1155**
o4xm03060	**1998 Aug 21**	**22:30:02**	**1.23**	**1155**
o4xm03070	1998 Aug 21	23:42:42	1.23	1145
o4xm03080	1998 Aug 22	00:05:17	1.23	1145

TABLE 2
ATOMIC DATA FOR SI

Multiplet	J_u	J_l	Actual λ (Å)	Transition Probability (s^{-1})	Oscillator Strength	Reference
$^5\mathbf{D}^0 \rightarrow {}^3\mathbf{P}$	...	...	...	...	...	...
...	3	2	1472.97	4.20×10^7	1.91×10^{-2}	1
...	2	2	1473.02	6.15×10^5	2.00×10^{-4}	2
...	1	2	1473.07	3.91×10^4	7.63×10^{-6}	2
...	2	1	1481.66	1.70×10^7	9.33×10^{-3}	1
...	1	1	1481.71	4.28×10^5	1.41×10^{-4}	2
...	0	1	1481.74	3.84×10^3	4.21×10^{-7}	2
...	1	0	1485.62	2.30×10^6	2.28×10^{-3}	1
$^3\mathbf{D}^0 \rightarrow {}^3\mathbf{P}$	...	...	**1478.50**	$\mathbf{1.65 \times 10^8}$	$\mathbf{9.01 \times 10^{-2}}$	**1**
...	3	2	1473.99	1.60×10^8	7.30×10^{-2}	1
...	2	2	1474.38	5.00×10^7	1.63×10^{-2}	1
...	1	2	1474.57	6.20×10^6	1.21×10^{-3}	1
...	2	1	1483.04	1.20×10^8	6.60×10^{-2}	1
...	1	1	1483.23	7.50×10^7	2.47×10^{-2}	1
...	1	0	1487.15	8.70×10^7	8.65×10^{-2}	1
$^3\mathbf{S}^0 \rightarrow {}^3\mathbf{P}$	...	...	**1813.73**	$\mathbf{5.67 \times 10^8}$	$\mathbf{9.33 \times 10^{-2}}$	**2**
...	1	2	1807.31	3.17×10^8	9.32×10^{-2}	2
...	1	1	1820.34	1.88×10^8	9.33×10^{-2}	2
...	1	0	1826.24	6.23×10^7	9.34×10^{-2}	2
$^5\mathbf{S}^0 \rightarrow {}^3\mathbf{P}$	...	...	...	...	...	...
...	2	2	1900.29	6.60×10^4	3.60×10^{-5}	3
...	2	1	1914.70	1.80×10^4	1.70×10^{-5}	3

REFERENCES.— (1) Morton 1991; (2) Tayal 1998; (3) Müller 1968.

TABLE 3
MEASURED FLUXES FOR SI

Multiplet	Central λ (Å)	STIS Flux* (10^{-3} photons cm^{-2} s^{-1})	IUE Flux*	FOS Flux*
^{5}**D**$^0 \rightarrow$ ^{3}**P**	**1479**	**0.51 ± 0.09**	···	···
···	1473.0	0.376 ± 0.083	···	···
···	1481.7	0.107 ± 0.027	···	···
···	1485.6	0.026 ± 0.007	···	···
^{3}**D**$^0 \rightarrow$ ^{3}**P**	**1479**	**0.76 ± 0.11**	···	···
···	1474.1	0.394 ± 0.059	···	···
···	1483.1	0.289 ± 0.087	···	···
···	1487.2	0.075 ± 0.019	···	···
^{3}**S**$^0 \rightarrow$ ^{3}**P**	**1814**	···	**5.4 ± 0.9**	**1.1 ± 0.2**
···	1807.3	···	1.7 ± 0.4	0.45 ± 0.08
···	1820.3	···	2.8 ± 0.4	0.50 ± 0.07
···	1826.2	···	0.5 ± 0.2	0.10 ± 0.03
^{5}**S**$^0 \rightarrow$ ^{3}**P**	**1900**	···	**5.1 ± 0.9**	**2.0 ± 0.2**
···	1900.3	···	3.8 ± 0.5	1.48 ± 0.09
···	1914.7	···	1.3 ± 0.4	0.43 ± 0.08

*Flux values are from entries in bold in Table 1.

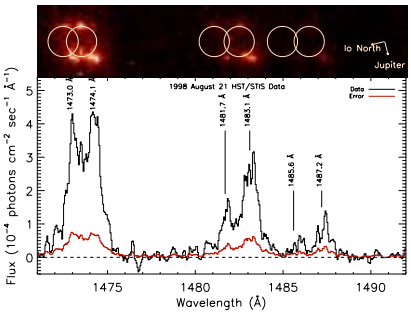

Fig. 1.— Data extracted from the sum of the first two HST/STIS G140M exposures in the near vicinity of Io. The multiplet components of the S I λ1479 emission are seen. The brightest emission is located at the anti- and sub-jovian equatorial spots (top) with the compass showing the direction of Jupiter and Io North. The flux spectrum corresponding to the sub-jovian spot is plotted (bottom) with the data in black and the propagated errors in red.

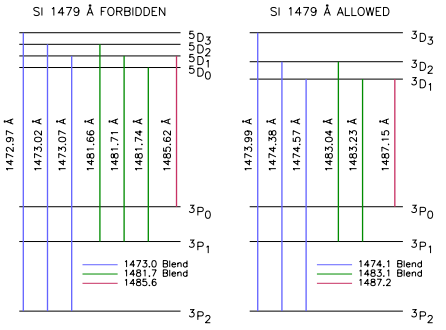

Fig. 2.— Grotrian diagram for the S I λ1479 dipole allowed and forbidden multiplets. All transition lines are shown. The lines indicated as blends are not individually resolved in the STIS data.

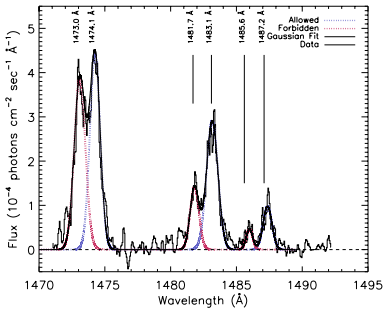

Fig. 3.— Synthetic fit to the flux spectrum of the STIS data previously shown in Fig. 1. The forbidden multiplet fit is in red, the allowed in blue, and the total fit in boldface black. The resolved transition lines and blends are indicated.

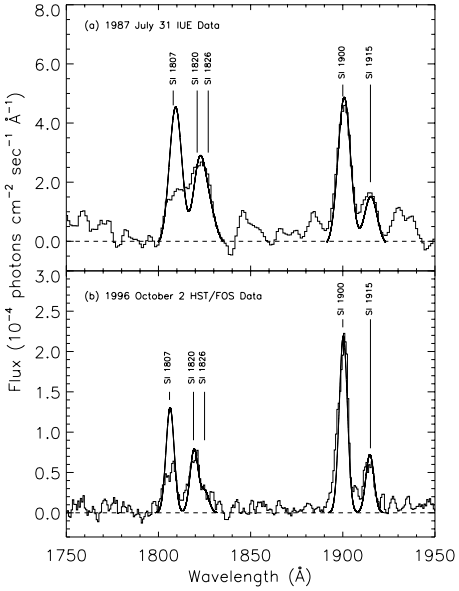

Fig. 4.— Flux spectra of Io's atmospheric emissions in the wavelength range 1750-1950 Å taken with (a) IUE and (b) HST/FOS. S I λ1814 and S I] λ1900 emissions are present and are overplotted with an optically thin profile of the multiplets in bold. The optically thin profile is normalized to the blend of the 1820 Å and the 1826 Å line. This comparison establishes that the S I] λ1900 transition is optically thin whereas S I λ1814 is optically thick.

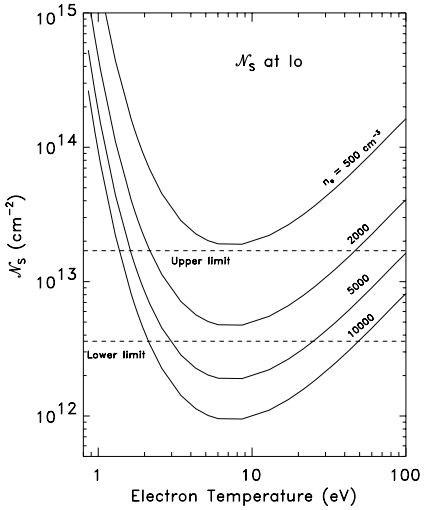

Fig. 5.— Several sulfur column density curves corresponding to different values of the electron density are plotted for the average measured brightness of S I] λ1900 taken from the IUE data with Io west of Jupiter. The upper and lower limits of the sulfur column density from our analysis of the STIS S I λ1479 data, $3.6\times10^{12}\,\mathrm{cm}^{-2} < \mathcal{N}_s < 1.7\times10^{13}\,\mathrm{cm}^{-2}$, are indicated by the dashed lines. The canonical T_e and n_e values of 5 eV and 2000 cm^{-3} give an $\mathcal{N}_s$ of $5\times10^{12}\,\mathrm{cm}^{-2}$, consistent with our bounds.

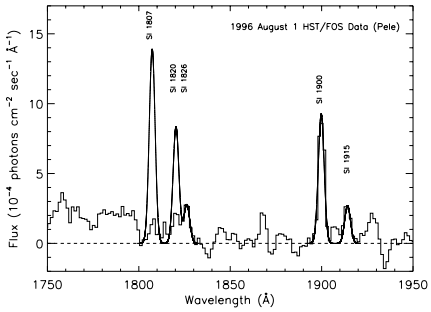

Fig. 6.— Pele volcano flux spectrum from McGrath et al. (2000). A synthetic fit for optically thin neutral sulfur emission, used to analyze the FOS data presented earlier in this paper, is overplotted on the data and is normalized to the 1826 Å line. This illustrates that the S I λ1814 multiplet experiences severe optical thickness effects while the S I] λ1900 doublet does not. This indicates that the sulfur column density is larger over Pele than the equatorial spots.